Applied Physics
Express

LETTER • OPEN ACCESS

Scintillation efficiency of Tb:$YTaO_4$ single crystals

To cite this article: Encarnación G. Víllora *et al* 2025 *Appl. Phys. Express* **18** 032002

OPEN ACCESS

Applied Physics Express 18, 032002 (2025) LETTER

https://doi.org/10.35848/1882-0786/adb89f

Scintillation efficiency of Tb:$YTaO_4$ single crystals

Encarnación G. Víllora[1*], Yueshen Zhou[1,2], Kenichi Watanabe[3], and Kiyoshi Shimamura[1,2*]

[1]National Institute for Materials Science, 1-1 Namiki, Tsukuba, Ibaraki, 305-0044, Japan
[2]Waseda University, 3-4-1 Ookubo, Shinjuku, Tokyo, 169-8555, Japan
[3]Kyushu University, 744 Motooka, Nishi-ku, Fukuoka, 819-0395, Japan

*E-mail: VILLORA.Garcia@nims.go.jp; SHIMAMURA.Kiyoshi@nims.go.jp

Received February 16, 2025; revised February 18, 2025; accepted February 19, 2025; published online March 12, 2025

Environmentally friendly scintillators are demanded to substitute $CdWO_4$ single crystal for *X*-ray imaging. Tb^{3+}:$YTaO_4$ single crystals are a promising candidate with a high stopping power, green emission matching to photodiodes, and a small afterglow. This study demonstrates that the light yield of Tb^{3+}:$YTaO_4$ scintillators is ~ 24,000 ph/MeV. Furthermore, the fluorescence lifetime, ~ 970 μs, though shorter than in other oxides, is close to the theoretical prediction by Judd-Ofelt analysis, indicating a high emission quantum efficiency of the Tb^{3+} activator. As the scintillation lifetime is shorter due to non-radiative decay, a potential light yield increase to 33,000 ph/MeV is estimated.

Supplementary material for this article is available online

$CdWO_4$ (CWO) is one of the earliest found and implemented scintillators still used for high-energy *X*-ray radiography applications.[1)] Its high density (ρ = 7.9 g cm^{-3}) and stopping power (estimated as ρ*Z_{eff}^4 = 134 × 10^6, with an effective atomic number Z_{eff} = 64.2), low afterglow (~ 0.01% @ 20 ms), and radiation resistance are unique. Though its light yield (LY) is moderate (~14,000 ph MeV^{-1}), its intrinsic visible emission matches well with the spectral sensitivity of Si-photodiodes (Si-PDs). The possibility of producing transparent CWO single crystals using the standard Czochralski growth technique is also crucial for the device implementation in bulk form. Despite various advantages, the toxic character of Cd is a fundamental drawback since environmentally friendly materials are being demanded in evolving worldwide directives. Therefore, there is a need to develop alternative materials to substitute CWO.

Terbium is one of the typical dopants in phosphors and scintillators. Its dominant green luminescence is used in fluorescent displays, *X*-ray and neutron imaging, radiation dosimetry, lasers, biological markers, etc.[2–12)] In the particular case of scintillators, Tb^{3+} represents an activator ion with a remarkable emission quantum efficiency (QE) in the visible, matching well the spectral sensitivity of Si-PDs. Furthermore, since its decay is comparatively slow, with a lifetime in the millisecond order, it is suitable for applications where sensitivity and spatial resolution, rather than dynamic response, are essential. The most representative example, which has become a commercial product, is Tb:Gd_2O_2S (Tb:GOS).[3,5,13–15)] It exhibits a high density and stopping power of Tb:GOS (7.34 g cm^{-3} and 102x10^6, respectively), and a high LY. However, only translucent ceramics can be synthesized, limiting its use to thin film applications. Recently, it has been shown that among the heavy tantalates, doped $YTaO_4$ (YTO) transparent single crystals are a promising alternative to CWO,[16,17)] particularly when doped with Tb. With a relatively high activator concentration, 15%Tb:YTO compromises high density and stopping power (7.76 g cm^{-3} and 129 × 10^6, respectively) with an emission maximum in *X*-ray luminescence (XRL). The radioluminescence LY of Tb:YTO, however, hasn't been determined yet because the decay of Tb^{3+} ions is too slow to carry out a standard pulse-height analysis (PHA).

This study aims to determine the LY of $Y_{1-x}Tb_xTaO_4$ (Tb:YTO, or 100·x%Tb:YTO) single crystals grown by the Floating zone (FZ) technique. Pulse area integration[18)] (PAI) is used to evaluate the LY instead of standard PHA. Furthermore, to assess the emission efficiency of Tb^{3+} activator ions, photoluminescence (PL) decay measurements upon intraatomic and conduction band excitation are measured and compared with theoretical values obtained through Judd-Ofelt (JO) analysis. By further comparison with the XRL decay, the scintillation efficiency is estimated.

Tb:YTO crystals were grown by the FZ technique using a four-xenon-lamp furnace from Crystal Systems Corp. The compositions were varied along the full solid-solution range, from low Tb concentrations up to fully substituted $TbTaO_4$ (TTO). High-purity (4 N) oxides (Y_2O_3, Ta_2O_5, and Tb_4O_7) were weighed in stoichiometric ratios and mixed. Feed rods were prepared by isostatic pressing at 300 MPa and subsequent sintering at 1300 °C for 10 h under a reducing Ar+3%H_2 atmosphere. Further growth details and grown crystals are shown in a previous publication.[17)] Here, it should be noted that the actual Tb concentration in crystals agreed with the nominal one according to energy-dispersive X-ray spectroscopy.

LY measurements were carried out by a digital PAI using a setup specially designed for scintillators with a decay time in the millisecond order.[18)] ^{137}Cs isotope was used as the excitation source, which emits 662 keV gamma photons upon intermediate beta decay to metastable ^{137}Ba of only 153 s half-life. The difference in spectral sensitivity of the photomultiplier for the emissions of Tb:YTO and BGO reference was corrected with the factor 2.026. Excitation and emission PL spectra were recorded with a Jasco-8600DS fluorescence spectrometer. PL decay measurements were obtained with a setup consisting of an oscilloscope, a chopper, a Fluorolog Jobin-Yvon photospectrometer from Horiba, and an R928 Hamamatsu photomultiplier. The continuous excitations sources were pulsed with a single narrow slit blade rotating at a frequency of 11.5 Hz. This

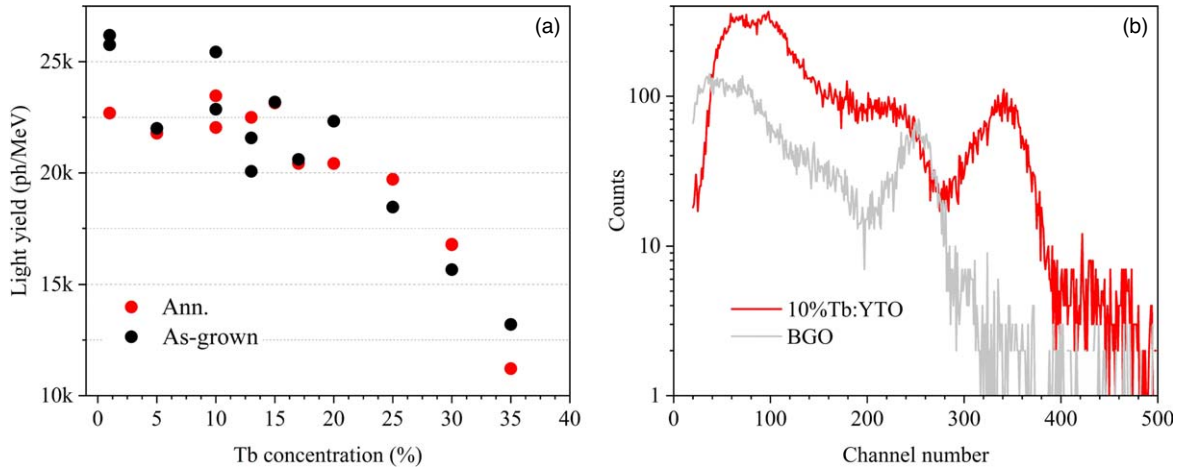

Fig. 1. (a) Light yield of Tb:YTO crystals as a function of Tb concentration. (b) ^{137}Cs γ-ray integrated pulse area response of representative 10%Tb:YTO and reference BGO.

guaranteed a long enough decay time between excitation pulses but promoted a slow rise time. While reabsorption was negligible due to the short penetration depth of excitation sources, emissions with wavelengths longer than that of excitation were selected with the spectrometer to prevent artifacts from scattered light. The 546 nm emission ($^5D_4 \rightarrow {}^7F_5$) decay was measured upon, firstly, intraatomic Tb^{3+} excitation ($^7F_6 \rightarrow {}^5D_4$ transition) with a 488 nm laser pointer, and, secondly, excitation in the conduction band of a host with a 222 nm lamp from Quark Technology (eVIO-100). The 437 nm emission ($^5D_3 \rightarrow {}^7F_4$) decay was measured upon intraatomic Tb^{3+} excitation ($^7F_6 \rightarrow {}^5D_3$ transition) with a UV LED (LED-UV365P from OptoCode Corp.). Transmittance measurements for the JO analysis were performed with a Jasco V-570 UV–vis-NIR spectrometer and a PerkinElmer Spectrum One FT/IR. The dispersion of the refractive index n from 231 to 800 nm was determined with an OPTM-A1 from Otsuka Electronics on a random crystal surface. It should be noticed that though the monoclinic crystals are optically biaxial, the anisotropy is supposed to be relatively small in these crystals.[16] Within the measured range (231 to 800 nm) n didn't show any systematical change with the Tb concentration, and even agreed well with reported values for YTO[19] and $GdTaO_4$[20] tantalates. Therefore, the n values in the near IR range were taken from the literature.

The LY of Tb:YTO crystals as a function of Tb concentration is shown in Fig. 1. The PAI analysis was carried out by comparison with the energy distribution response of a $Bi_4Ge_3O_{12}$ (BGO) single crystal of 8,000 ph/MeV LY under the same experimental conditions. Up to 20% Tb content, the LY of all samples lies between 20,000 and 26,000 ph MeV^{-1}, i.e. within the $\sim$ 10% standard deviation inherent to the PAI technique. This value is about 70% higher than that of a standard CWO. Beyond 25%Tb concentration, the LY rapidly decreases, and reliable measurements above 35% Tb couldn't be conducted under the same conditions. The LY drop with Tb concentration was equally observed in prior measurements of integrated XRL spectra, and it was attributed to quadrupole-quadrupole interactions between neighboring Tb^{3+} ions.[17] Unlike former XRL measurements, there is no noticeable improvement after annealing under a reducing atmosphere, nor is there a clear maximum LY at 15%Tb concentration. If the annealing effect is only superficial, the difference between both results might be attributed to the largely differing penetration depth of both excitation sources. While 8 keV Cu X-rays are absorbed at the surface (within $< 100\,\mu$m) in former XRL, gamma-rays in current PAI pass through the sample (penetration depth $\sim$ 10 cm). Therefore, the homogeneity of the annealing process requires a further detailed investigation.

The PL decay of Tb^{3+} ions upon dissimilar excitation paths, namely intraatomic @ 488nm and through host @ 222nm, was investigated to gain more insight into the emission efficiency. The distinction between both excitation wavelengths is understandable when considering the PL spectra. Figure 2(a) shows the excitation and emission PL of 15%Tb:YTO and TTO along with the spectra of the YTO host reference. At the same time, Fig. 2(b) illustrates the Tb^{3+} energy levels relative to the valence and conduction bands of the YTO host. As found by XPS,[21] the valence band of YTO, mainly determined by O-2p orbitals, broadens by the appearance of Tb^{3+} energy levels after Tb incorporation, where the ground state $^7F_6$ represents the new valence band maximum. As a result, the 5.0 eV bandgap of YTO narrows to the 4.0 eV one of TTO. Consequently, three excitation possibilities can be distinguished: (1) a pure Tb^{3+} intraatomic absorption at 488 nm, the well-known $^7F_6 \rightarrow {}^5D_4$ transition, (2) a Tb^{3+}-host absorption peaking at 280 nm, the transition $^7F_6 \rightarrow$ Ta-5d from the Tb^{3+} ground level at the valence band maximum to the conduction band bottom, and (3) the host absorption peaking at 222 nm, in good correspondence with the non-doped YTO excitation maximum.

The results of PL decay measurements are shown in Fig. 3. The PL decay curves are characterized by a single exponential component, independently of both the excitation wavelength and the Tb concentration. The decay curves of 15%Tb:YTO and TTO with the corresponding fitting are shown as examples in Fig. 3(b). This finding contrasts with the double exponential decay observed in previously measured XRL curves.[17] The lifetime dependences on Tb content upon the host and intraatomic excitation are very similar to the former dependence of the slow XRL component. However, their absolute values are different. The three curves exhibit the longest lifetime for the 15%Tb:YTO crystal, indicating that the non-

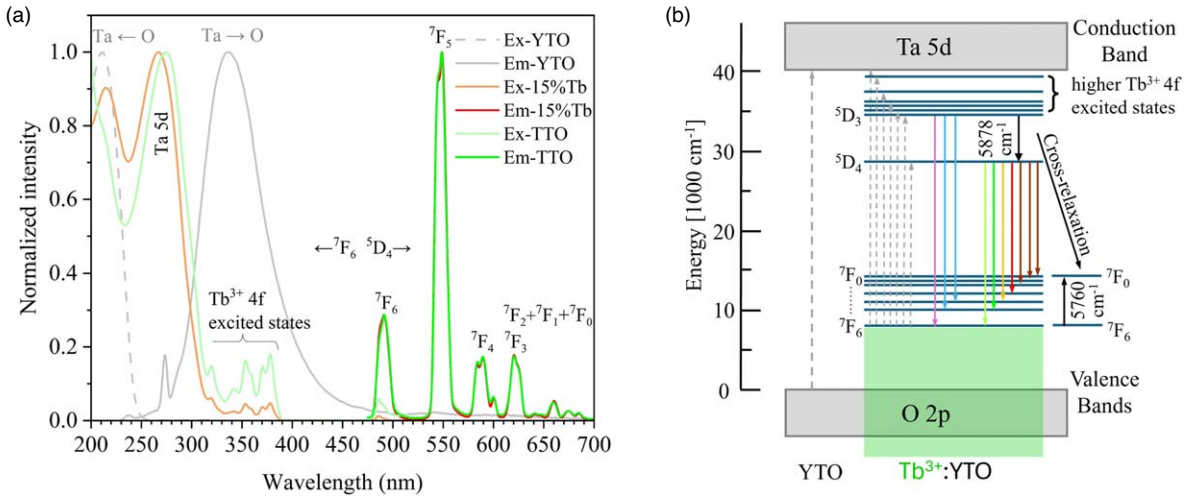

Fig. 2. (a) Excitation & emission PL spectra of 15%Tb:YTO and TTO, together with YTO host reference. (b) Schematic energy diagram of Tb^{3+}:YTO.

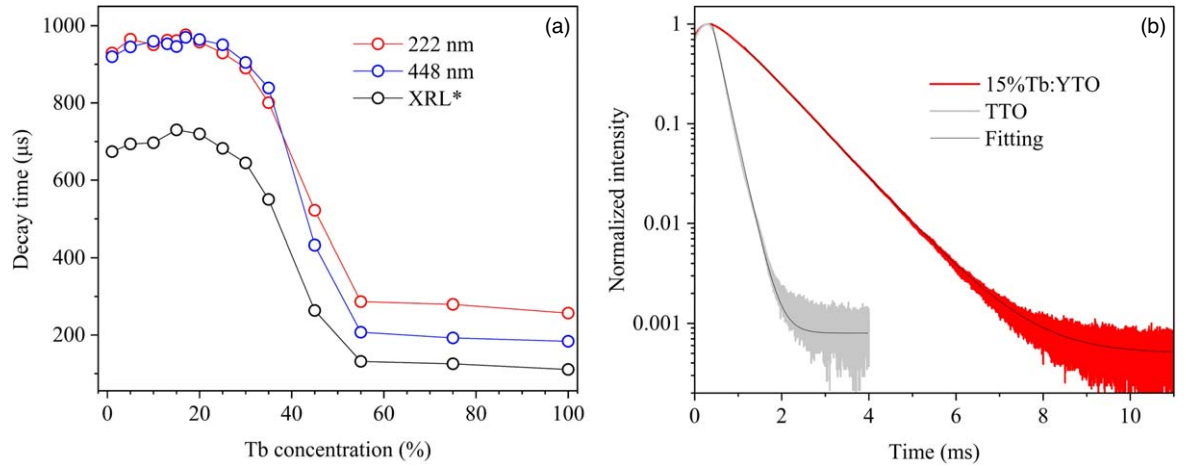

Fig. 3. (a) Lifetime of Tb:YTO crystals upon excitation in the UV (host @ 222 nm) & visible (intraatomic @ 488 nm) as a function of Tb concentration. (b) Decay curves of 15%Tb:YTO and TTO upon UV excitation. *[17].

radiative recombination losses are minimal at this concentration. This finding completely correlates with the maximum LY observed in integrated XRL measurements. Following the same logic, the lifetimes decrease when the quadrupole-quadrupole Tb interactions quench the luminescence at higher concentrations. The following observations are made by comparison of the absolute values: (1) in the low Tb concentration range, the lifetimes upon intraatomic and host excitations are the same, indicating an optimum electronic transfer from the conduction band to the Tb^{3+} activator ions. (2) On the contrary, in the high Tb concentration range, the lifetime upon excitation into the conduction band is higher, indicating that the probability of non-radiative recombination of excited electrons is lower. Under the hypothesis of a homogeneous excitation of all Tb^{3+} centers upon intraatomic excitation, the latter observation indicates that the conduction band favors the transfer of excited electrons to radiative Tb^{3+} centers, lessening the transfer to non-radiative ones. (3) Upon excitation in the upper energy bands by high-energy ionizing radiation (*X*- or γ-rays), there is a general decrease in lifetime for all Tb concentrations, caused by non-radiative recombination losses. In other words, the LY can be improved. To evaluate the scintillation potential of Tb:YTO crystals, a detailed investigation of the theoretical transition probabilities *A*, branching ratios β, and radiative lifetimes τ_R of excited Tb^{3+} energy levels in Tb:YTO crystals was approached for the first time by the JO formalism.

In the free-ion approximation, the $4f^n$ electric dipole transition (ED) intensity from an initial ground state of quantum numbers (*S, L, J*) to an excited state of quantum numbers (*S', L', J'*) is theoretically estimated by

$$S_{ED}(J;J') = \sum_{t=2,4,6} \Omega_t \, |\langle f^n[SL]J \, \|U^{(t)}\| \, f^n[S'L']J'\rangle|^2, \quad (1)$$

where $U^{(t)}$ are the host independent doubly reduced matrix elements of rank *t*, and Ω_t (t = 2, 4, 6) the JO parameters specific to the material. The JO analysis relies on accurately determining the absorption spectrum $\alpha(\lambda)$. For each state (or manifold m), the mean wavelength is calculated as $\bar{\lambda} = \int \lambda\alpha(\lambda)d\lambda / \int \alpha(\lambda)d\lambda$, the absorption cross-section as $\bar{\Gamma} = \int \alpha(\lambda)d\lambda/[Tb]$, and the resulting line strength as

$$S_m = \frac{3ch(2J+1)}{8\pi^3 e^2 \bar{\lambda}} n \left(\frac{3}{n^2+2}\right)^2 \bar{\Gamma}, \quad (2)$$

where *n* is the refractive index, *c* the speed of light, and *h* the Planck's constant. The JO parameters are determined by the

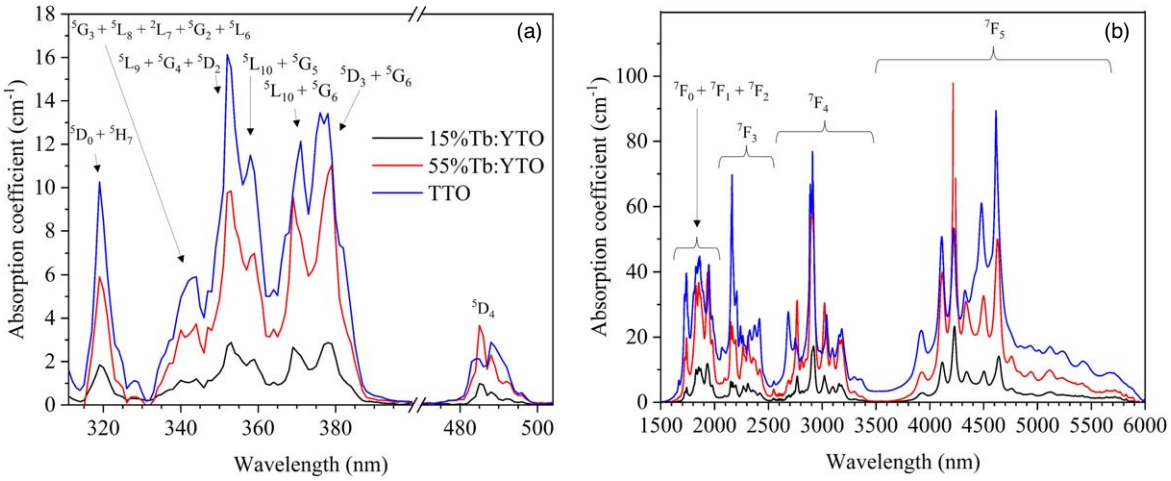

Fig. 4. Absorption coefficient of Tb^{3+} in the (a) UV-visible and (b) near IR wavelength regions of 15% and 55%Tb:YTO, and TTO crystals.

least-square fitting that minimizes the difference between the theoretical (Eq. (1)) and experimental (Eq. (2)) line strengths.[22)]

Though magnetic dipole interactions (MD) are generally orders of magnitude smaller than ED ones, their contributions are sometimes non-negligible. Their line strengths are calculated as.[23)]

$$S_{MD}(J;J') = \mu_B^2 \,|\langle f^n[SL]J \,\|L + 2S\|\, f^n[S'L']J'\rangle|^2, \quad (3)$$

and the resulting transition probabilities $A(J;J')$ as

$$A(J;J') = \frac{64\pi^4 e^2}{3h(2J'+1)\bar{\lambda}^3}\left[n\left(\frac{n^2+2}{3}\right)^2 S_{ED} + n^2 S_{MD}\right], \quad (4)$$

The radiative lifetime τ_R and the emission branching ratio β of an excited state J' are obtained from the $A(J;J')$ as

$$\tau_R = \frac{1}{\sum_J A(J;J')} \quad (5)$$

and

$$\beta = \frac{A(J;J')}{\sum_J A(J;J')}. \quad (6)$$

The transmittance spectra of representative crystals, namely 15% and 55%Tb:YTO, and the fully substituted TTO, were measured. The derived absorption coefficient of Tb^{3+} as a function of wavelength in the UV-visible-near IR is shown in Fig. 4, where the corresponding Tb^{3+} $4f^n$ excited states are indicated. The absorption cross-sections were calculated considering the Tb concentrations of the crystals (20.33, 73.89, and 133.00 $\times$ 10^{-20} atoms/cm^3 for 15%, 55%, and 100%Tb, respectively).

The experimental and JO calculated line strengths are summarized in Table I for three well-differentiated Tb concentrations: 15% and 55%Tb:YTO, and fully substituted TTO. The least-square fittings of the absorption bands are relatively good, as indicated by the small δ values. The obtained JO parameters Ω_t (t = 2, 4, and 6) are very similar for the evaluated samples despite the largely varying Tb content, contrasting with the shifts observed with composition.[24–28)] The Ω_t dependences observed in glasses are attributed to the modification in the local structure with the composition, the Ω_2 being particularly dependent on covalency and asymmetry .[25,27)] As in the case of Tb:YTO, the Tb site remains invariant along the whole solid solution between YTO and TTO compounds, it is reasonable that Ω_t are comparable within the errors of the semiempirical JO approximation. The calculated Ω_t are relatively close to those of a Tb-doped lithium borate glass.[26)]

Table II summarizes the JO estimation of transition probabilities, branching ratios, and radiative lifetimes of the metastable $^5D_3$ and $^5D_4$ energy levels of Tb^{3+} for the representative case of 15%Tb:YTO. For comparison, the experimental lifetimes and branching ratios of 1% and 15%Tb:YTO obtained by PL are also given. For the greenish emission from the $^5D_4$ level, the agreement between experimental and calculated results is reasonably good. Instead, the approximation of the bluish emission from the upper $^5D_3$ level is less accurate. The PL emission and decay stemming from the $^5D_3$ level are displayed in Fig. 5. There is a noteworthy difference in the most intense transitions; for 1%Tb:YTO, it is the $^5D_3 \rightarrow {}^7F_6$, while the estimated is the $^5D_3 \rightarrow {}^7F_4$. Furthermore, the fluorescent lifetime τ_{PL}, 440 μs from a single exponential decay, is 70% of the radiative τ_R with a value of 630 μs. The suppression of the bluish emission at relatively low Tb concentrations is well-known and attributed to a cross-relaxation process,[29–31)] as shown in the scheme of Fig. 2(b). The energy is transferred by the emission $^5D_3 \rightarrow {}^5D_4$ from an excited Tb^{3+} ion and the subsequent absorption $^7F_6 \rightarrow {}^7F_0$ at a neighboring one in the ground state. This process is resonant and accelerates the depopulation of the $^5D_3$ level, quenching the bluish emission by shortening its lifetime. Meanwhile, it favors the increase in the greenish emission by the population of the $^5D_4$ level.[31,32)] Additionally, it should be noticed that the observation of the bluish emission in Tb:YTO crystals is indicative of a homogeneous Tb distribution in the rare earth site since the presence of Tb clusters would quench the emission.

A comparison of the JO calculation with other Tb-doped single crystals is given in Table III. Tb-fluorides exhibit lower Ω_2 values and longer lifetimes than Tb-oxides. The small covalency characteristic of fluorides causes the low Ω_2. The Ω_t values of Tb:YTO crystals are within the typical range for oxides, however, their lifetimes are relatively shorter. The Ω_2 of $TbAlO_3$ seems to be overestimated, particularly when compared with the analogous to our case Tb:$YAlO_3$. The measured PL decay of Tb:YTO crystals in the lower concentration range is pretty close to the radiative one estimated by JO,

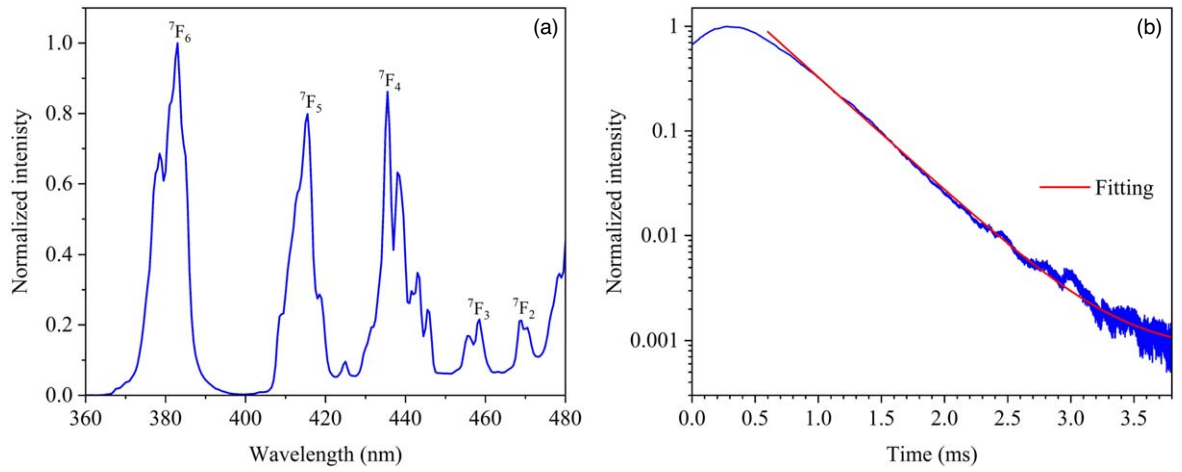

Fig. 5. (a) PL emission and (b) decay from the Tb^{3+} $^5D_3$ excited state of 1%Tb:YTO.

Table I. Measured and calculated average absorption line strengths of 15%Tb:YTO, 55%Tb:YTO, and TTO. Derived JO parameters Ω_t and root-mean-square deviations δ.

$[Tb^{3+}]$ =	15% Tb:YTO			55% Tb:YTO			TTO		
Transition $^7F_6 \rightarrow$	$\bar{\lambda}$ (nm)	Line strength (10^{-20} cm^2)		$\bar{\lambda}$ (nm)	Line strength (10^{-20} cm^2)		$\bar{\lambda}$ (nm)	Line strength (10^{-20} cm^2)	
		S(exp.)	S(calc.)		S(exp.)	S(calc.)		S(exp.)	S(calc.)
$^5H_7+^5D_0$	319.5	0.0898	0.0866	319.6	0.0671	0.0815	319.6	0.0653	0.0754
$^5G_2+^5G_3+^5L_6+^5L_7+^5L_8$	342.0	0.1232	0.1262	342.6	0.0000	0.1254	343.2	0.0931	0.1131
$^5L_9+^5G_4+^5D_2$	352.8	0.1324	0.1832	352.4	0.0922	0.183	352.2	0.0767	0.1638
$^5G_5+^5L_{10}$	359.4	0.0961	0.2397	358.8	0.1289	0.2382	358.1	0.1024	0.2142
$^5L_{10}+^5G_6$	369.6	0.1208	0.2471	369.7	0.1098	0.2455	370.0	0.0701	0.2198
$^5G_6+^5D_3$	378.2	0.1740	0.0689	378.1	0.1708	0.0678	376.5	0.1752	0.0596
$^5D_4$	487.1	0.0351	0.0135	486.6	0.0374	0.0127	487.8	0.0270	0.0116
$^7F_0+^7F_1+^7F_2$	1877.4	3.2801	3.214	1873.0	3.2730	3.2116	1856.2	2.8121	2.8709
$^7F_3$	2263.0	1.9301	2.087	2261.4	1.9921	2.1123	2252.2	2.0799	1.7897
$^7F_4$	2958.9	3.2971	3.2152	2956.6	3.2608	3.1992	2967.3	2.5164	2.6732
$^7F_5$	4565.3	6.1340	6.1472	4539.8	5.7463	5.7558	4606.3	5.1599	5.1335
Ω_2 ($\times$ 10^{-20} cm^2) =		6.6 ± 0.4			5.7 ± 0.4			5.6 ± 0.5	
Ω_4 ($\times$ 10^{-20} cm^2) =		3.5 ± 0.3			3.6 ± 0.3			2.8 ± 0.3	
Ω_6 ($\times$ 10^{-20} cm^2) =		3.08 ± 0.11			3.07 ± 0.11			2.76 ± 0.15	
δ ($\times$ 10^{-20} cm^2) =		0.104			0.105			0.146	

Table II. Calculated line strengths S, transition probabilities A, branching ratios β, and radiative lifetimes τ_R of $^5D_3$ and $^5D_4$ energy levels of Tb^{3+} for the representative 15%Tb:YTO crystal. Experimental branching ratios β_{PL} and fluorescent lifetimes τ_{PL} of 1% and 15%Tb:YTO crystals are given for comparison.

Transition	λ (nm)	S (x10^{-20} cm^2)	A_{ED} (s^{-1})	A_{MD} (s^{-1})	β	τ_R (ms)	1%Tb:YTO		15%Tb:YTO	
							β_{PL}	τ_{PL} (ms)	β_{PL}	τ_{PL} (ms)
$^5D_3 \rightarrow {}^5D_4$	1725.9	0.4867	83.16	60.201	0.090				—	
$^7F_0$	484.7	0	0	0	0.000				—	
$^7F_1$	479.5	0.0122	108.375	0	0.068		0.009		—	
$^7F_2$	469.3	0.0184	175.028	40.747	0.135		0.019		—	
$^7F_3$	454.7	0.0085	89.472	2.208	0.058		0.035		—	
$^7F_4$	435.4	0.0433	527.259	144.961	0.421		0.276		—	
$^7F_5$	412.8	0.0183	265.367	0	0.166		0.261		—	
$^7F_6$	380.8	0.0052	98.571	0	0.062	0.63	0.401	0.440	—	—
$^5D_4 \rightarrow {}^7F_0$	673.9	0.0061	14.235	0	0.016		0.016		0.017	
$^7F_1$	664	0.0089	21.963	0	0.025		0.019		0.020	
$^7F_2$	644.6	0.0092	24.778	0	0.028		0.008		0.009	
$^7F_3$	617.4	0.0187	57.674	14.31	0.082		0.092		0.092	
$^7F_4$	582.3	0.0136	50.307	0.453	0.058		0.116		0.115	
$^7F_5$	542.6	0.1047	485.517	122.756	0.691		0.578		0.576	
$^7F_6$	488.6	0.0135	87.746	0	0.100	1.14	0.172	0.929	0.171	0.976

Table III. Comparison of JO parameters Ω_t (t = 2, 4, and 6) ($\times 10^{-20}$ cm^2), and radiative τ_R and PL τ_{PL} lifetimes of Tb^{3+} in various crystals (* glass).

Crystal	Ω_2	Ω_4	Ω_6	τ_R (ms)	τ_{PL} (ms)	References
15%Tb:YTO	6.6	3.5	3.08	1.14	0.976	this work
55%Tb:YTO	5.7	3.6	3.07	1.23	0.286	"
TTO	5.6	2.8	2.76	1.3	0.257	"
3%Tb:30Li_2O·70B_2O_3 *	5.56	1.33	3.22	—	—	26)
5%Tb:CaF_2	1.71	2.65	2.25	6.77	6.06	33)
$LiTbF_4$	1.5	2.23	2.06	6.8	3.8	34)
$Tb_{0.81}Ca_{0.19}F_{2.81}$	1.14	1.52	1.82	6.9	4.2	34)
TbP_5O_{14}	3.77	1.7	3.43	3.82	3.4	35)
$TbLiP_4O_{12}$	3.5	2.43	1.8	4.09	3.7	35)
$Ba_3Tb(PO_4)_3$	2.53	8.55	1.3	3.54	3.17	36)
$TbAl_3(BO_3)_4$	8.15	0.29	2.44	2.07	0.8	35)
7%Tb:$Na_3La_9O_3(BO_3)_8$	1.05	11.74	1.59	2.38	2.02	37)
1%Tb:$KYb(WO_4)_2$	0.86	1.66	1.98	2.08	0.395	38)
0.1%Tb:$YAlO_3$	3.25	7.13	2	2.07	1.71	39)
7%Tb:$Y_3Al_5O_{12}$	2.75	0.12	3.37	3.3	3.12	40)
Tb:$YAlO_3$	3.49	5.87	2.55	2.31	1.72	41)
$TbAlO_3$	40.52	8.74	2.26	3.5	2	42)
Tb:Lu_2O_3	3.79	1.3	1.08	3.02	1.13	43)
$Tb_3Sc_2Al_3O_{12}$	4.47	1.37	4.23	—	—	44)

Supplementary table. Calculated line strengths S, transition probabilities A, branching ratios β, and radiative lifetimes τ_R of all Tb^{3+} energy levels for the representative 15%Tb:YTO crystal.

suggesting that the emission QE of the Tb^{3+} center is quite high. The fluorescence QE η can be approximately estimated with the theoretical radiative decay as

$$\eta = \frac{\tau_{measured}}{\tau_R}. \quad (7)$$

Therefore, for the optimum 15%Tb:YTO, with τ_{PL} & τ_{XRL} values of 976 and 730 μs, respectively, the η_{PL} and η_{XRL} are ~86% and 64%, respectively. It is noteworthy that the fluorescence efficiency in Tb:YTO is quite high up to the concentration quenching above 20%Tb, suggesting that the resonant energy transfer is negligible.[31] From this it can be deduced that the scintillation LY has a potential improvement of about ~36%, increasing from ~24,000 ph/MeV to 33,000 ph MeV^{-1}, if the non-radiative recombination centers that quench the scintillation are eliminated.

The present study evaluates the scintillation LY of FZ-grown Tb:YTO transparent single crystals by PAI technique. Up to 20%Tb, the LY is in the order of 24,000 ph MeV^{-1}, i.e. ~70% brighter than standard CWO. The measured PL decay time of the green luminescence is close to 1 ms, which is in good agreement with the theoretical estimation by JO analysis. By further comparison with the XRL decay, an LY improvement of ~36%, reaching 33,000 ph MeV^{-1}, is expected upon eliminating or neutralizing non-radiative recombination centers. This result proves the potential of Tb:YTO single crystals to substitute CWO in high-energy *X*-ray imaging applications.

Acknowledgments The authors would like to express their sincere thanks to Dr. Yuichi Oshima for his kind help with the refractive index measurements and to Mr. Satoshi Yamamoto for his support with the polishing of various crystals.

1) T. Yanagida, "Inorganic scintillating materials and scintillation detectors," Proc. Jpn. Acad. Ser. B **94**, 5 (2018).
2) W. W. Moses, "Scintillator requirements for medical imaging," SCINT99LBNL-45805.
3) X. Yan, G. R. Fern, R. Withnall, and J. Silver, "Effects of the host lattice and doping concentration on the colour of Tb^{3+} cation emission in of $Y_2O_2S:Tb^{3+}$ and $Gd_2O_2S:Tb^{3+}$ nanometer sized phosphor particles," Nanoscale **5**, 8640 (2013).
4) I. Kandarakis and D. Cavouras, "Experimental and theoretical assessment of the performance of Gd_2O_2S:Tb and La_2O_2S:Tb phosphors and Gd_2O_2S:Tb-La_2O_2S:Tb mixtures for X-ray imaging," Eur. Radiol. **11**, 1083 (2001).
5) S. Chen, L. J. Li, J. Chen, S. Xu, W. Huang, Z. Wen, T. Jiang, and H. Guo, "Highly resolved and refreshable X-ray imaging from Tb^{3+} doped aluminosilicate oxyfluoride glass scintillators," J. Mat. Chem. C **11**, 2389 (2023).
6) N. Ali and P. D. Sahare, "Dosimetry characteristics of $NaLi_2PO_4:Tb^{3+}$ OSLD phosphor," J. Radioanal. Nucl. Chem. **330**, 941 (2021).
7) M. Sen, R. Shukla, N. Pathak, K. Bhattacharyya, V. Sathian, P. Chaudhury, M. S. Kulkarni, and A. K. Tyagi, "Development of $LiMgBO_3:Tb^{3+}$ as a new generation material for thermoluminescence based personnel neutron dosimetry," Mater. Adv. **2**, 3405 (2021).
8) L. Chen, Y. Wu, H. Huo, B. Tang, X. Ma, J. Wang, C. Sun, J. Sun, and S. Zhou, "Nanoscale Gd_2O_2S:Tb scintillators for high-resolution fluorescent imaging of cold neutrons," ACS Appl. Nano Mater. **5**, 8440 (2022).
9) H. Tanaka, S. Kalusniak, M. Badtke, M. Demesh, N. V. Kuleshov, F. Kannari, and C. Kränkel, "Visible solid-state lasers based on Pr^{3+} and Tb^{3+}," Prog. Quantum Electron. **84**, 100411 (2022).
10) B. Tang, W. Yin, Q. Wang, L. Chen, H. Huo, Y. Wu, H. Yang, C. Sun, and S. Zhou, "High quantum efficiency rare-earth-doped Gd_2O_2S:Tb, F scintillators for cold neutron imaging," Molecules **28**, 1815 (2023).
11) D. Nakauchi, K. Watanabe, T. Kato, N. Kawauchi, and T. Yanagida, "Scintillation light yield of Tb-doped Lu_2O_3 single crystals," Nucl. Instrum. Methods Phys. Res. B **546**, 165167 (2024).
12) T. Wang, R-F. Huang, and Z. Chen, "Ultra-sensitive Tb^{3+}/G-quadruplex fluorescence detection of oxidative DNA damage coupled with DNA glycosylase," Microchem. J. **201**, 110734 (2024).
13) Y. Tian, W-H. Cao, X-X. Luo, and Y. Fu, "Preparation and luminescence property of Gd_2O_2S:Tb X-ray nano-phosphors using the complex precipitation method," J. Alloys Compd. **433**, 313 (2007).
14) R. Yasuda, M. Katagiri, and M. Matsubayashi, "Influence of power particle size and scintillator layer thickness on the performance of Gd_2O_2S:Tb scintillators for neutron imaging'.," Nucl. Instrum. Methods Phys. Res. A **680**, 139 (2012).
15) J. Crha, J. Vila-Comamala, E. Lehmann, C. David, and P. Trtik, "Light yield enhancement of 157-gadolinium oxysulfide scintillator screens for the high-resolution neutron imaging," MethodsX **6**, 107 (2019).
16) Y. Zhou, D. Yuan, E. G. Víllora, D. Nakauchi, T. Kato, N. Kawaguchi, T. Yanagida, and K. Shimamura, "High-density Nb:$YTaO_4$ single crystals or X-ray scintillation," Cryst. Eng. Comm. **27**, 81 (2025).
17) Y. Zhou, D. Yuan, E. G. Víllora, D. Nakauchi, N. Kawaguchi, T. Yanagida, and K. Shimamura, "High performance $Y_{1-x}Tb_xTaO_4$ single-crystal scintillators for X-ray detection," Cryst. Growth Des. **25**, 359 (2025).
18) K. Watanabe, T. Yanagida, D. Nakauchi, and N. Kawaguchi, "Scintillation light yield of Tb:$Sr_2Gd_8(SiO_4)_6O_2$," Jpn. J. Appl. Phys. **60**, 106002 (2021).
19) Z. Ma, J. Zheng, S. Wang, and L. Gao, "First-principle calculations of crystal structures, electronic structures, and optical properties of $RETaO_4$ (RE=Y, La, Sm, Eu, Dy, Er)," Opt. Eng. **57**, 017107 (2018).

20) S. Ding, A. Kinross, X. Wang, H. Yang, Q. Zhang, W. Lie, and D. Sun, "Experiment and density functional theory analyses of $GdTaO_4$ single crystal," Solid State Commun. **273**, 5 (2018).
21) Y. Zhou, E. G. Víllora, R. Sahara, A. Saengdeejing, and K. Shimamura, submitted manuscript.
22) B. M. Walsh "Judd-Ofelt theory: principles and practicesed. B. Di Bartolo and O. Forte, *Advances in Spectroscopy for Lasers and Sensing* (Springer, Berlin, 2006), 10.1007/1-4020-4789-4_21.
23) B. M. Walsh, N. P. Barnes, and B. Di Bartolo, "Branching ratios, cross sections, and radiative lifetimes of rare Earth ions in solids: application to Tm^{3+} and Ho^{3+} ions in $LiYF_4$," J. Appl. Phys. **83**, 2772 (1998).
24) M. Zahir, R. Olazcuaga, C. Parent, G. Le Flem, and P. Hagenmuller, "A structural interpretation of the Pb^{2+}, Eu^{3+} and Nd^{3+} optical spectra in doped sodium borate glasses," J. Non-Cryst. Solids **69**, 221 (1985).
25) S. Tanabe, T. Ohyagi, N. Soga, and T. Hanada, "Compositional dependence of Judd-Ofelt parameters of Er^{3+} ions in alkali-metal borate glasses," Phys. Rev. B **46**, 3305 (1992).
26) H. Takebe, Y. Nageno, and K. Morinaga, "Compositional dependence of judd-ofelt parameters in silicate, borate, and phosphate glasses," J. Am. Ceram. Soc. **78**, 1161 (1995).
27) H. Ebendorff-Heidepriem and D. Ehrt, "Tb^{3+} f-d absorption as indicator of the effect of covalency on the Judd-Ofelt Ω_2 parameter in glasses," J. Non-Cryst. Solids **248**, 247 (1999).
28) M. M. Naaim, N. N. Yusof, E. S. Sazali, M. N. Azlan, S. M. Iskandar, and R. Hisam, "Effect of mixed TeO_2-B_2O_3 glass former in Ho^{3+}/Yb^{3+}-doped glass system: Raman spectroscopy, Judd-Ofelt and luminescence investigations," Ceram. Int. **50**, 18497 (2024).
29) D. J. Robbins, B. Cockayne, B. Lent, and J. L. Glasper, "The mechanism of $^5D_3$-$^5D_4$ cross-relaxation in $Y_3Al_5O_{12}$:Tb^{3+}," Solid State Commun. **20**, 673 (1976).
30) B. C. Jamalaiah, M. V. Vijaya Kumar, and K. Rama Gopal, "Investigation on luminescence and energy transfer in Tb^{3+}-doped lead telluroborate glasses," Physica B **406**, 2871 (2011).
31) G. R. Dillip, C. M. Reddy, M. Rajesh, S. Chaurasia, B. Deva, P. Raju, and S. W. Joo, "Green fluorescence of terbium ions in lithium fluoroborate glasses for fiber lasers and display devices," Bull. Mater. Sci. **39**, 711 (2016).
32) A. A. da Silva, M. A. Cebim, and M. R. Davolos, "Excitation mechanisms and effects of dopant concentration in Gd_2O_2S:Tb^{3+}," J. Lumin. **128**, 1165 (2008).
33) J. Liu, Z. Shi, Q. Song, D. Li, N. Li, Y. Xue, J. Xu, J. Xu, Q. Wang, and X. Xu, "Judd-Ofelt analysis and spectroscopic study of Tb:CaF_2 and Tb/Pr:CaF_2 co-doped single crystals," Opt. Mater. **108**, 110219 (2020).
34) V. Vasyliev, Encarnación, G. Víllora, Y. Sugahara, and K. Shimamura, "Judd-Ofelt analysis and emission quantum efficiency of Tb-fluoride single crystals: $LiTbF_4$ and $Tb_{0.81}Ca_{0.19}F_{2.81}$," J. Appl. Phys. **113**, 203508 (2013).
35) S. Colak and W. Z. Zwicker, "Transitions rates of Tb^{3+} in TbP_5O_{14}, $TbLiP_4O_{12}$, and $TbAl_3(BO_3)_4$: an evaluation for laser applications," J. Appl. Phys. **54**, 2156 (1983).
36) H. Chen, P. Loiseau, G. é. Aka, and C. Kränkel, "Optical spectroscopy investigation of $Ba_3Tb(PO_4)_3$ single crystals for visible laser applications," J. Alloys Compd. **740**, 1133 (2018).
37) F. Shan, G. Zhang, X. Zhang, T. Xu, Y. Wu, Y. Fu, and Y. Wu, "Growth and spectroscopic properties of Tb^{3+}-doped $Na_3La_9O_3(BO_3)_8$ crystal," J. Cryst. Growth **424**, 1 (2015).
38) P. Loiko et al., "Judd-Ofelt modelling and stimulated-emission cross-sections for Tb^{3+} ions in monoclinic $KYb(WO_4)_2$ crystal," J. Lumin. **190**, 37 (2017).
39) M. J. Weber, T. E. Varitimos, and B. H. Matsinger, "Optical intensities of rare-earth ions in yttrium orthoaluminate," Phys. Rev. B **8**, 47 (1973).
40) J. Liu, Q. Song, D. Li, Y. Ding, X. Xu, and J. Xu, "Spectroscopic properties of Tb:$Y_3Al_5O_{12}$ crystal for visible laser application," Opt. Mater. **106**, 110001 (2020).
41) B. Liu et al., "Crystal growth, polarized spectroscopy and Judd-Ofelt analysis of Tb:$YAlO_3$," Spectrochim. Acta A Mol. Biomol. Spectrosc. **200**, 58 (2018).
42) D. K. Sardar, K. L. Nash, R. M. Yow, and J. B. Gruber, "Absorption intensities and emission cross sections of Tb^{3+} ($4f^8$) in $TbAlO_3$," J. Appl. Phys. **100**, 083108 (2006).
43) J. Shi et al., "Crystal growth and spectral properties of Tb:Lu_2O_3," Chin. Phys. B **27**, 097801 (2018).
44) S. Ding, H. Zhang, R. Dou, W. Liu, D. Sun, and Q. Zhang, "Theoretical and experimental studies of electronic, optical and luminescent properties of Tb-based garnet crystals," J. Solid State Chem. **263**, 123 (2018).